JOURNAL OF GEOPHYSICAL RESEARCH, VOL. 103, NO. E9, PAGES 20,217–20,236, AUGUST 30, 1998

Hubble Space Telescope imaging of Jupiter's UV aurora during the Galileo orbiter mission

John T. Clarke,[1] Gilda Ballester,[1] John Trauger,[2] Joe Ajello,[2] Wayne Pryor,[3] Kent Tobiska,[2] J.E.P. Connerney,[4] G. Randall Gladstone,[5] J.H. Waite Jr.,[5] Lotfi Ben Jaffel,[6] and Jean-Claude Gérard[7]

Abstract. Hubble Space Telescope (HST) Wide-Field Planetary Camera 2 (WFPC 2) images of Jupiter's aurora have been obtained close in time with Galileo ultraviolet spectrometer (UVS) spectra and in situ particles, fields, and plasma wave measurements between June 1996 and July 1997, overlapping Galileo orbits G1, G2, G7, G8, and C9. This paper presents HST images of Jupiter's aurora as a first step toward a comparative analysis of the auroral images with the in situ Galileo data. The WFPC 2 images appear similar to earlier auroral images, with the main ovals at similar locations to those observed over the preceding 2 years, and rapidly variable emissions poleward of the main ovals. Further examples have been observed of the equatorward surge of the auroral oval over 140-180^0 longitude as this region moves from local morning to afternoon. Comparison of the WFPC 2 reference auroral ovals north and south with the VIP4 planetary magnetic field model suggests that the main ovals map along magnetic field lines exceeding $15R_J$, and that the Io footprint locations have lead angles of 0-10^0 from the instantaneous magnetic projection. There was an apparent dawn auroral storm on June 23, 1996, and projections of the three dawn storms imaged with HST to date demonstrate that these appear consistently along the WFPC 2 reference oval. Auroral emissions have been consistently observed from Io's magnetic footprints on Jupiter. Possible systematic variations in brightness are explored, within factor of 6 variations in brightness with time. Images are also presented marked with expected locations of any auroral footprints associated with the satellites Europa and Ganymede, with localized emissions observed at some times but not at other times.

1. Introduction

Jupiter's auroras have previously been imaged at ultraviolet, X ray, and near-infrared wavelengths, with related thermal emissions imaged at longer infrared wavelengths. The early auroral observations have been reviewed elsewhere [*Clarke et al.*, 1989] and the more recent observations are summarized in the following references. The ionospheric H_3^+ IR emissions [*Drossart et al.*, 1989; *Drossart et al.*, 1992; *Trafton et al.*, 1989; *Kim et al.*, 1991; *Kim et al.*, 1994; *Baron et al.*, 1991; *Connerney et al.*, 1993; *Connerney et al.*, 1996] display a similar morphology to the directly excited UV emissions [*Broadfoot et al.*, 1979; *Clarke et al.*, 1980; *Clarke et al.*, 1995b; *Clarke et al.*, 1996; *Skinner et al.*, 1984; *Livengood et al.*, 1992; *Caldwell et al.*, 1992; *Dols et al.*, 1992; *Gérard et al.*, 1993; *Gérard et al.*, 1994; *Prangé et al.*, 1995; *Harris et al.*, 1996; *Grodent et al.*, 1996]. The X ray emissions [*Metzger et al.*, 1983; *Waite et al.*, 1994] have a different morphology, with the emissions extending to low latitudes, and the thermal IR emissions [*Kostiuk et al.*, 1977; *Caldwell et al.*, 1980; *Caldwell et al.*, 1988; *Drossart et al.*, 1986] are as yet poorly understood.

Jupiter's UV aurora exhibit main emission ovals which are aligned about the north and south magnetic poles and corotate with the planet at the System III (magnetic) rotation period, in contrast with Earth's auroral pattern, which appears generally fixed with respect to the solar wind direction. In addition to this general pattern, there are pronounced variations of Jupiter's auroral emissions along these ovals, and there are significant motions of the emissions with respect to the time-averaged oval locations. One example of this is a tendency for the emissions in the morning sector to

[1]Department of Atmospheric, Oceanic, and Space Science, University of Michigan, Ann Arbor.
[2]Jet Propulsion Laboratory, Pasadena, California.
[3]Laboratory for Atmospheric and Space Physics, University of Colorado, Boulder.
[4]NASA Goddard Space Flight Center, Greenbelt, Maryland.
[5]Southwest Research Institute, San Antonio, Texas.
[6]Institute for Astrophysics, Paris, France.
[7]Institute of Astrophysics, University of Liège, Liège, Belgium.

Paper number 98JE01130.
0148-0227/98/98JE-01130$09.00

Table 1. HST/WFPC 2 Images of Jupiter's Aurora During the Galileo Orbiter Mission

Date	UT	Expo-. sure, s	WFPC 2 Obsroot	Jupiter CML, deg	Io OLG, deg	Galileo Orbit	Galileo Region	Galileo Distance, R_J	Panel in Plate 2
June 23.1996	1501	500	u3b10302	210.7	304.7	G1	dawn	48	a
June 23.1996	1515	600	u3b10303	219.7	306.9	G1	dawn	48	
June 23.1996	0354	600	u3b10202	318.6	54.9	G1	morning	44	b
June 24.1996	1344	400	u3b10102	314.3	138.0	G1	morning	39	
June 24.1996	1359	500	u3b10103	323.9	140.2	G1	morning	39	
June 24.1996	1507	500	u3b1a102	5.0	149.8	G1	morning	39	c
June 24.1996	1521	600	u3b1a103	14.0	151.9	G1	morning	39	
June 24.1996	1653	400	u3b1a109	68.6	164.5	G1	morning	39	c
June 24.1996	1707	600	u3b1a10a	78.1	166.7	G1	morning	39	
June 24.1996	1819	500	u3b1a10c	121.1	176.7	G1	morning	39	d
June 24.1996	1833	600	u3b1a10d	130.1	178.8	G1	morning	39	
June 24.1996	2006	500	u3b1a10j	185.8	191.7	G1	morning	39	e
June 24.1996	2023	600	u3b1a10k	196.6	194.2	G1	morning	39	
June 24.1996	2132	600	u3b1a10m	238.3	203.9	G1	morning	39	
June 24.1996	2148	600	u3b1a10n	248.0	206.1	G1	morning	39	
June 27.1996	1534	500	u3b10502	113.4	44.6	G1	afternoon	12	f
June 27.1996	1548	600	u3b10503	122.3	46.7	G1	afternoon	12	
June 28.1996	0114	500	u3b10602	104.0	126.6	G1	afternoon	11	g
June 28.1996	0128	600	u3b10603	113.0	128.7	G1	afternoon	11	
June 29.1996	2353	400	u3b10402	355.9	162.0	G1	post-dusk	27	h
June 30.1996	0005	600	u3b10403	4.2	163.9	G1	post-dusk	27	
Sept. 3, 1996	0938	500	u3fw0502	58.1	156.2	G2	morning	44	i
Sept. 3, 1996	0952	600	u3fw0503	67.1	158.3	G2	morning	44	
Sept. 7, 1996	1144	500	u3fw0202	16.1	267.8	G2	afternoon	11	j
Sept. 7, 1996	1158	600	u3fw0203	25.1	270.0	G2	afternoon	11	
Sept. 7, 1996	1457	500	u3fw0302	132.8	295.3	G2	afternoon	11	k
Sept. 7, 1996	1511	600	u3fw0303	141.8	297.4	G2	afternoon	11	
Sept. 8, 1996	1014	500	u3fw0402	112.2	99.1	G2	post-dusk	16	l
Sept. 8, 1996	1028	600	u3fw0403	121.2	101.2	G2	post-dusk	16	
March 31, 1997	0155	500	u3b10702	238.4	102.0	G7	dawn	45	a'
March 31, 1997	0209	600	u3b10703	247.4	104.1	G7	dawn	45	
May 6, 1997	1051	500	u3fw0604	219.2	298.6	G8	pre-dawn	27	b'
May 6, 1997	1105	600	u3fw0605	228.8	300.7	G8	pre-dawn	27	
May 6, 1997	1541	500	u3fw0704	34.5	339.3	G8	pre-dawn	25	c'
May 6, 1997	1555	600	u3fw0705	43.5	341.4	G8	pre-dawn	25	
July 3, 1997	0608	500	u43b0101	142.3	181.5	C9	post-dusk	56	d'
July 3, 1997	0622	600	u43b0102	151.3	183.6	G9	post-dusk	56	
July 3, 1997	1429	500	u3b1a701	85.3	251.8	C9	post-dusk	58	e'
July 3, 1997	1443	600	u3b1a702	94.2	253.9	G9	post-dusk	58	
July 4, 1997	0803	600	u43b0202	3.0	41.2	C9	post-dusk	63	f'
July 4, 1997	0819	600	u43b0203	12.7	43.4	G9	post-dusk	63	
July 28, 1997	1748	500	u43b0402	12.4	329.7	C9	midnight	137	g'
July 28, 1997	1802	600	u43b0403	21.4	331.8	G9	midnight	137	
July 30, 1997	1320	500	u43b0302	151.7	339.1	C9	midnight	139	h'
July 30, 1997	1334	600	u43b0303	160.7	341.2	G9	midnight	139	

CML is System III longitude of the central meridian, OLG is orbital longitude from superior orbital conjunction, each for the midpoint of the exposure. Panels denoted by primes are from Plate 2b (1997 images); others are from Plate 2a (1996 images).

In each image pair close in time, the first was with filter F160BW, and the secondwith F160BW plus the CaF_2 blocking filter F130LP.

appear confined along the main oval, while the emissions spread widely in latitude in the afternoon sector, and one longitudinal region appears to move equatorward as it passes from local morning to local afternoon (the so-called "equatorward surge"). While the general structure of Jupiter's magnetosphere is known, due to the uncertainties in the planetary magnetic field models, it has not been possible to accurately "map" the main oval emissions into the magnetosphere in order to correlate them with the different regions and processes. We present here a comparison of the auroral ovals with an improved magnetic field model, derived in part from the observed latitudes of Io's footprint aurora.

In addition to the main ovals, there are more variable emissions observed poleward of the main ovals, and localized emissions associated with the satellite Io, which have been identified with Io through their persistent appearance near the expected locations of Io's magnetic footprints. There are also at times fainter emissions extending equatorward of the main oval to the observed

latitude of the Io footprint emissions, but no emissions have been detected equatorward of the mapping of Io's torus even after a careful modeling and subtraction of the disk emission. While some characteristic patterns and/or motions have been observed in the auroral emissions, the increasing number of images at different epochs now makes it possible to more clearly identify the persistent characteristics of Jupiter's aurora, as presented below.

The presence of the Galileo spacecraft in its orbital tour of Jupiter now makes it possible to compare Wide-Field Planetary Camera 2 (WFPC 2) images of Jupiter's UV aurora with in situ measurements of the magnetospheric plasma, magnetic field, energetic particles, and plasma waves. At the time of writing of this paper, systematic analyses of the particle and field data have not yet been presented, due in no small part to the large quantity of data collected during the 10 orbital encounters of the primary Galileo orbiter mission. In this paper we present UV images of Jupiter's aurora obtained with the Hubble Space Telescope (HST) WFPC 2 camera during periods of Galileo orbiter measurements of Jupiter's UV emissions and various properties of Jupiter's magnetosphere, along with an updated analysis of the properties of Jupiter's aurora now available from 3 years of WFPC 2 UV images. This is intended as a first step toward the comparative analysis of the auroral images with in situ data from the Galileo orbiter.

2. Observations and Data Reduction

FUV images of Jupiter have been obtained with the HST WFPC 2 between June 1996 and July 1997 (Table 1), overlapping Galileo orbits G1, G2, G7, G8, and C9. The characteristics of the WFPC 2 instrument [*Trauger et al.*, 1994; *Holtzman et al.*, 1995; *Clarke et al.*, 1995a] and the methods of reduction of the UV images [*Clarke et al.*, 1995b; *Clarke et al.*, 1996] have been presented previously. The response of the WFPC 2 with filter F160BW to Jupiter's auroral spectrum (Figure 1 and Plate 1) includes the H_2 Lyman ($B^1\Sigma_u^+ - X^1\Sigma_g^+$) band emissions and part of the Werner ($C^1\Pi_u - X^1\Sigma_g^+$) band series plus the H Ly α line. Inclusion of the F130LP filter blocks the H Ly α emission and Werner bands, and such images were obtained in each observation to facilitate cosmic ray identification and to isolate the Ly α emission from the difference of images. The response to Jupiter's auroral spectrum has been modeled (Figure 1) by convolving an IUE spectrum of the north aurora with the HST + WFPC 2 + filter band passes. The conversion to absolute brightness is based on mean WFPC 2 sensitivity curves allowing for degradation with time after decontamination cycles. For the assumed auroral spectrum, brightnesses have been estimated in each band pass using average sensitivity values of 0.00057 and 0.00050 electrons/s per WF pixel for 1 kR emissions with F160BW and F160BW+F130LP, and a sensitivity degradation of 40% in 30 days after each decontamination. These values were unchanged after the HST refurbishment mission and subsequent recomissioning of the WFPC 2 in February 1997, except for a temporarily higher rate of contamination in March 1997.

While the auroral emissions are produced in Jupiter's thermosphere, the WFPC 2 images sample Jupiter's upper atmosphere over altitudes ranging from the stratosphere to the thermosphere. In the F160BW band pass of 1150-2100 Å, the altitude of line of sight optical depth unity ranges from 50 km altitude (0.1 bar pressure) at 2100 Å (determined by H_2 Rayleigh scattering and NH_3

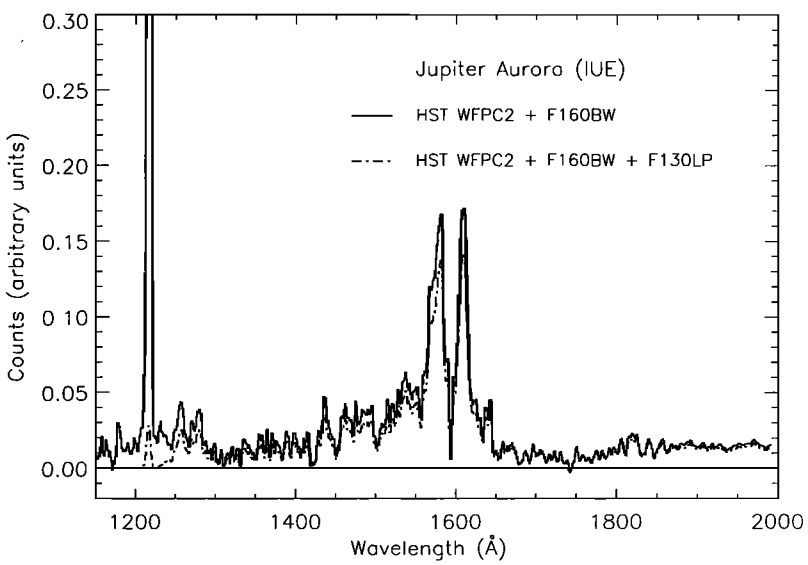

Figure 1. IUE spectrum of Jupiter's north aurora convolved with the HST + WFPC 2 response functions for two filters used in UV auroral imaging. The inclusion of the F130LP filter made of CaF_2 mainly blocks the H Ly α and short wavelength Werner band emissions. There is a small but real contribution from reflected solar continuum over 1750-2100 Å.

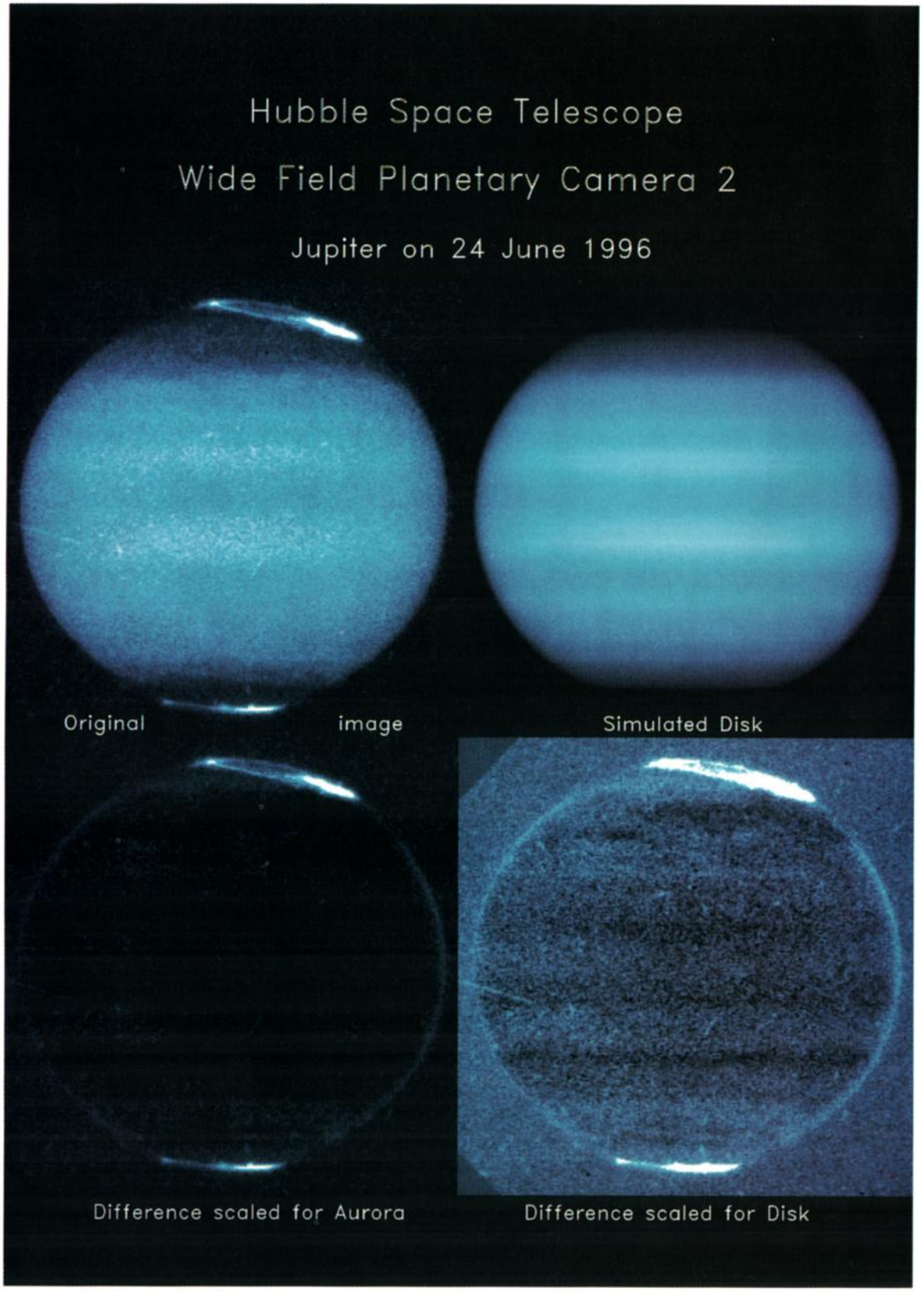

Plate 1. One example of the modeling and subtraction of the disk emission from Jupiter in an HST WFPC 2 filter F160BW image. The disk emission from the original image, upper left, has been modeled as described in the text, upper right, and then subtracted from the original image, lower left and right. This image is u3b1a10m taken on June 24, 1996, beginning at 2132 UT for 600 s. Note the remnant cosmic ray blemishes in the difference frames, as well as some deviations from the mean latitudinal banding pattern. The residual noise level is in the range 0.5 - 0.8 DN, and up to 2 times higher at the limb.

and aerosol extinction) to 300-400 km (1-10 μbar) below 1450 Å (from increasingly strong CH_4 photoabsorption). An independent analysis of the auroral emission spectrum indicates that overlying H_2 column densities of 10^{16} - 10^{20} cm^{-2} are required to explain the observed self-absorption, corresponding to altitudes of 400-1600 km [*Ajello et al.,* 1998]. The diffuse disk emission is dominated by scattered solar continuum at the longer wavelengths. The effective wavelength of the nonauroral light in the FUV images has been estimated by folding an IUE small-aperture spectrum of Jupiter's equator with the instrument response. For filter F160BW we derive a band pass with half power points at 1760 and 2070 Å and a central wavelength of 1900 Å, with a negligible contribution from light above 2200 Å. The observed limb darkening has been modeled analytically using a Minnaert law formulation with empirical coefficients [*West et al.,* 1995] with coefficients optimized for Jupiter's mid-latitude regions for the F160BW band pass. One example of the disk model and subtraction is shown in Plate 1. The mean north/south intensity pattern has been derived from images taken in May 1994, March 1995, June 1996, and July 1997 with filters F160BW + F165LP, which block the auroral emissions from below 1650 Å. From these inputs plus a convolution with the WFPC 2 point spread function, we have constructed simulated solar reflection disk images for the time of each observation (Plate 1). The absolute pointing has then been determined by minimizing the difference between the observed and simulated images. For the F160BW images, we estimate positional uncertainties on Jupiter of ~300 km projected area, comparable to the angular resolution. Jupiter's rotation results in image smear of about 1^0 of rotation per 100 s exposure time, degrading the resolution by the exposure length independently of the instrument resolution.

Since the main auroral ovals rotate with the planet, but also display systematic motions in addition to this rotation, we found it expedient to establish reference oval locations as a basis for comparison with the different images. We therefore created reference ovals [*Clarke et al.,* 1996] for both poles from WFPC 2 images showing complete ovals on March 24, 1995 (north), and March 4, 1995 (south). These reference locations are overplotted in Plates 2 and 3 for the start and end of each exposure and in Plates 4, 5, and 6 for the midpoint of each exposure, in all cases projected to an altitude of 400 km above the 1 bar level. They are also plotted in Figure 2 for comparison with the VIP 4 planetary magnetic field model [*Connerney et al.,* 1998]. This shows the degree of rotational blurring at different locations, and the observed deviations of emissions from the reference ovals are discussed below. Coordinate systems used in this paper are System III longitude and planetocentric latitude, and the "limb" refers to the altitude of the 1 bar pressure level, assuming an equatorial radius of 71,492 km and an oblateness of 0.06487. Since the apparent size of Jupiter as observed from Earth changes with time, we have scaled the angular extent of all the images displayed in this paper to a standard scale corresponding to a distance of 4.2000 AU from Jupiter.

3. Results and Discussion

The HST WFPC 2 images of Jupiter's aurora from June 1996 through July 1997 are presented in Plates 2 and 3. For each figure panel, the date, image number, and Galileo orbiter location are indicated in Table 1, along with Jupiter's central meridian longitude (CML) and the orbital longitude of Io. Note the repeated appearance of the three main features of Jupiter's aurora: the main ovals, diffuse emission poleward of the ovals (at times confused with the main ovals), and the Io footprint. In addition, the extent in altitude of the auroral curtain above the limb of the planet is clearly seen in many panels in Plate 2 as compared with the displayed altitude of the reference ovals of 400 km above the 1 bar level. The observed vertical extent of the emission is of the order of 1000-2000 km, several times greater than the uncertainty in pointing, and more detailed modeling of the altitude distribution of the Chapman layer of auroral emission is in progress. While the apparent brightness near the limb is increased by the slant path through the optically thin auroral emissions, there are also significant brightness variations observed along the main ovals at different times, and as reported earlier, the north and south emissions appear conjugate within the limits imposed by the observing geometry.

The spectral character of the different auroral emission features has been explored by comparing the pairs of images with and without the CaF_2 blocker F130LP, which effectively blocks emissions from below 1300 Å including the H Ly α line and the H_2 Werner band emissions. The ratio of emissions above and below 1300 Å in part indicates the degree of atmospheric absorption, principally by CH_4 and C_2H_2, of the escaping auroral emissions, and this is referred to as the "auroral color ratio" [*Yung et al.,* 1982]. In addition, the ratio of WFPC 2 images provides information on the ratio of H Ly α to H_2 band emissions. Since the mixing ratio of H atoms is expected to increase relative to H_2 molecules with increasing altitude in the auroral atmosphere, the WFPC 2 filter color ratio also provides information about the atmospheric composition, the altitude profile of the emissions, and possible contributions to the auroral emission of atomic excitation processes which do not have accompanying molecular emissions, such as energetic proton charge exchange, fast H atom collisions, and resonant scattering. In this sense, the analysis of the WFPC 2 filter color ratios requires accompanying spectra for an unambiguous interpretation, and HST Goddard High Resolution Spectrograph (GHRS) spectra have been obtained close in time to some of the WFPC 2 images listed in Table 1. A full analysis of these data is in progress, and will be reported at a later date.

One further complication in estimating the WFPC 2 filter color ratio on a spatial scale of 0.1 arc sec is the rapid rotation of Jupiter, which considerably alters the appearance of the auroral emission distribution over the typical 600 s. exposure. The direct shifting and division of subsequent auroral images yield a poorly registered resulting image, and more detailed modeling of

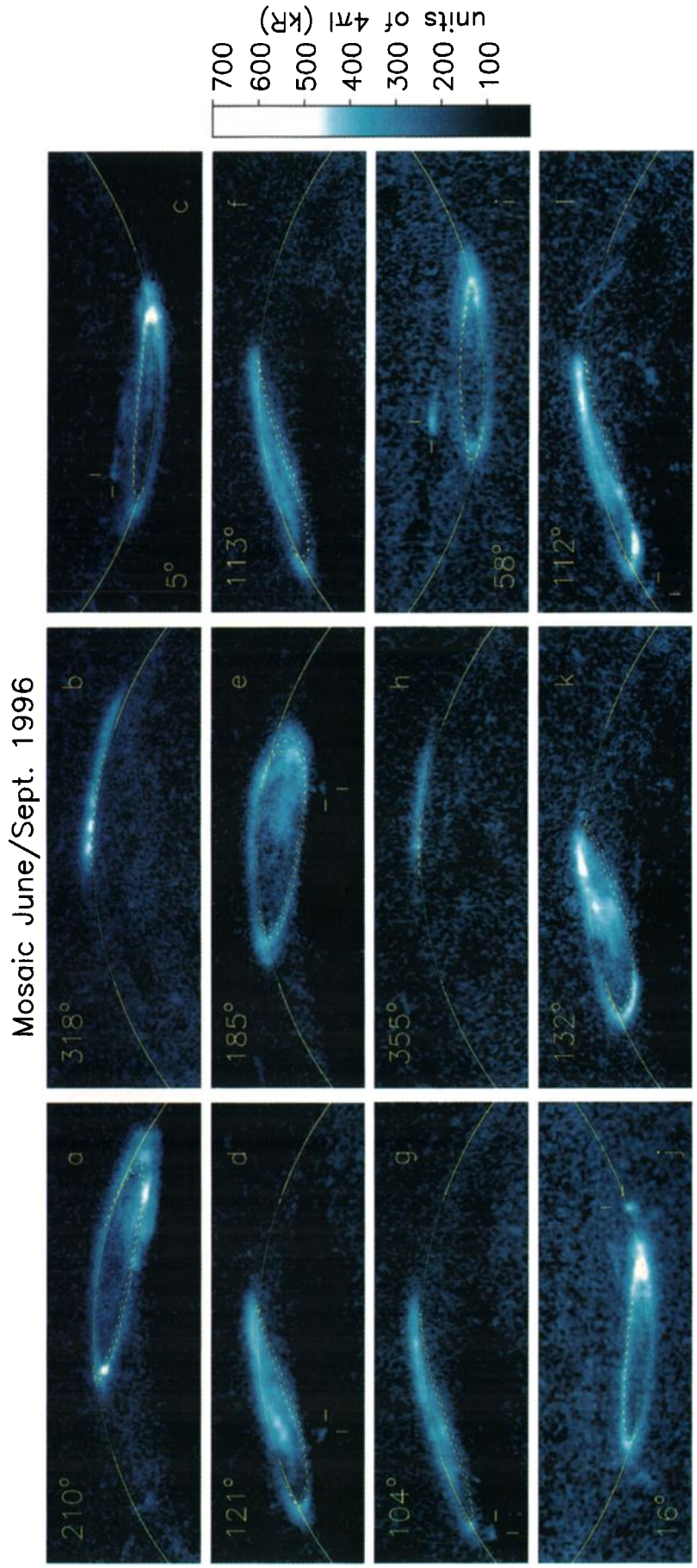

Plate 2a. WFPC 2 UV images of Jupiter's aurora in each observing period during the Galileo orbits G1 and G2 in June/September 1996. Panel letters are listed in Table 1, for more information about the observing times and conditions, and numbers indicate the CML at the midpoint of the exposure. The overplotted dashed lines are the WFPC 2 reference ovals at the beginning and end of each exposure, and each image plotted was with filter F160BW. The Io footprint appears in panels c, d, e, g, i, j, and l, as indicated with tick marks, and Jovian north is up in all panels.

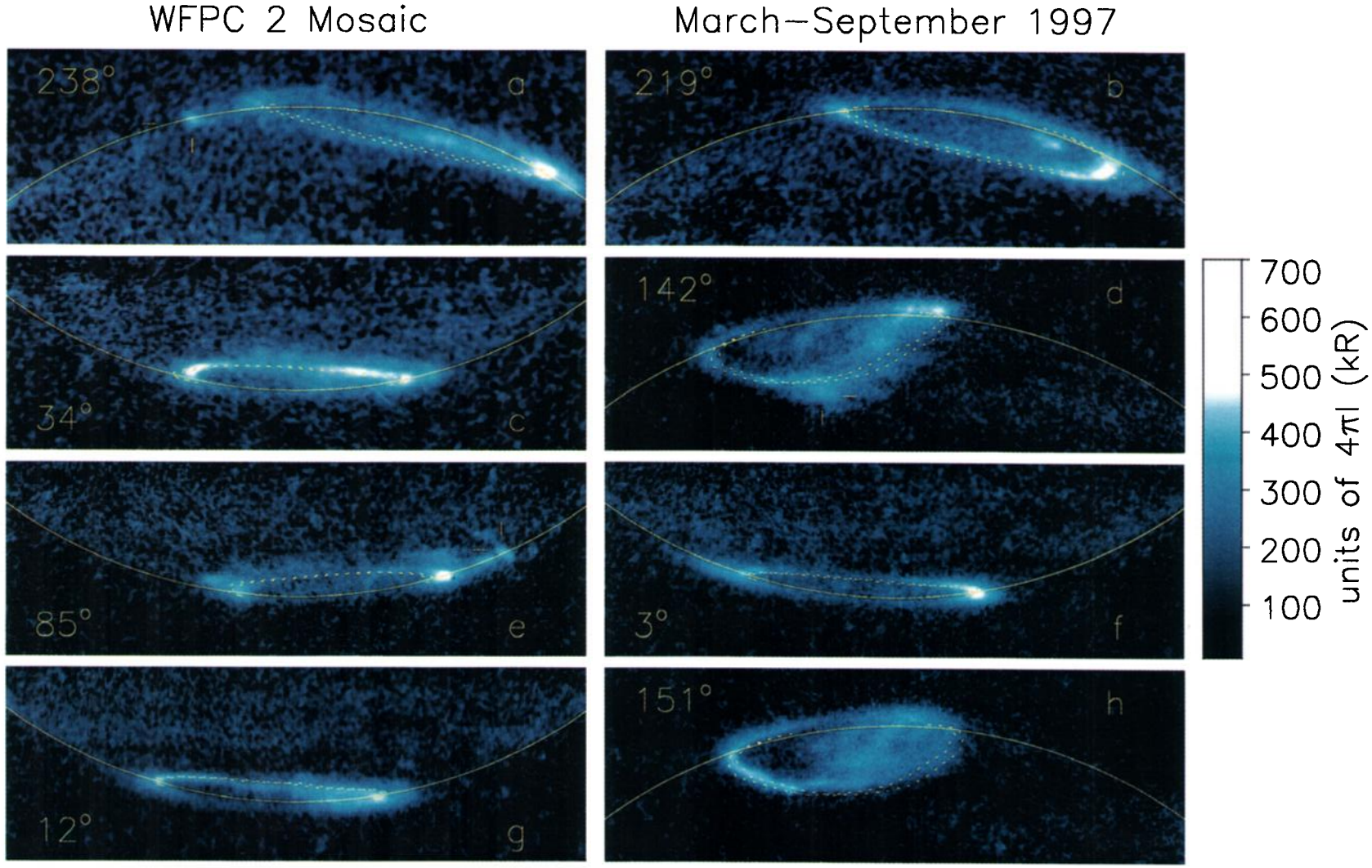

Plate 2b. WFPC 2 UV images of Jupiter's aurora during Galileo orbits G7, G8, and C9 over March - July 1997 with same notations as Plate 2a. The equatorward surge can be seen in progress in panels d and h, while the main oval has moved down to the reference oval latitude in panels a and b. Note the unusual double emission structure at low latitudes near the dusk limb in panel e; only one of these is the Io footprint, indicated with tick marks.

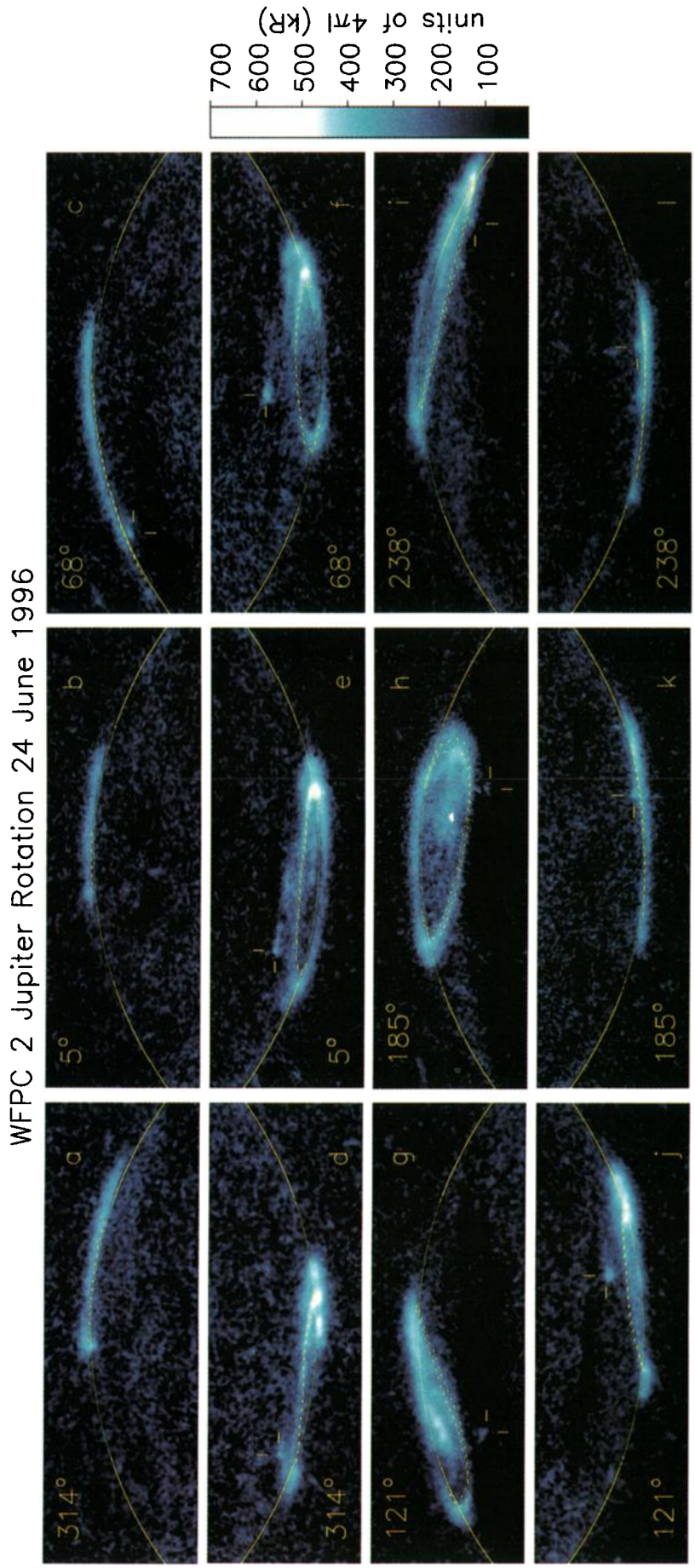

Plate 3. WFPC 2 UV images of Jupiter's aurora covering one complete Jovian rotation on June 24, 1996, with same notations as in Plate 2. Images with the same CML value show the N and S polar regions in the same image, and the sequence shows the evolution of the north and south aurora over one complete Jovian rotation. Note the relative brightening at the dusk limb, particularly in the southern aurora, throughout the rotation of the planet. The east/west motions of the Io footprint emission, which is visible in each image, are dominated by the changing mapping of the magnetic field from Io to Jupiter's atmosphere, resulting from Jupiter's rotation and the nondipolar nature of the magnetic field.

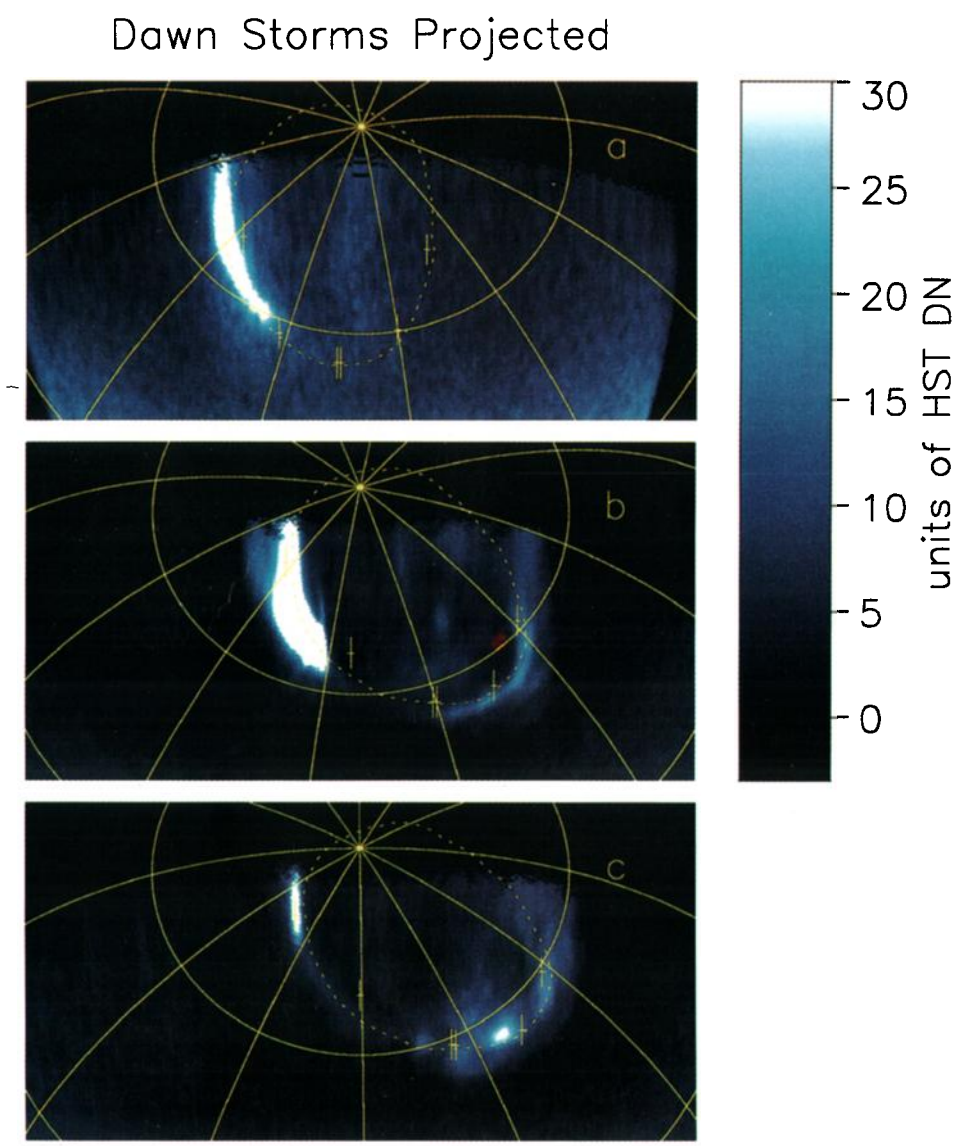

Plate 4. Jupiter's dawn auroral storms from three HST imaging observations, projected to a uniform point of view from above the central meridian and $+60^0$ latitude. Details of the three images are listed in Table 2. The dashed line in each panel indicates the WFPC 2 reference oval at the midpoint of the exposure, and the hatch marks overplotted on each reference oval indicate the locations of magnetic local dawn, 0300 hours, noon (double hatch marks), 1500 hours, and dusk. The dawn storm emissions can be seen to be close to the reference oval on each occasion, with a significant spreading in longitude which in each case also covers magnetic local dawn. In each case the bright emission extends to the limb, and its extent onto the nightside is unknown.

the altitude and spatial distributions of the emissions will be necessary to determine the filter color ratio of the auroral emissions on a 0.1 arc sec scale. In general, though, the filter color ratio of the Io footprint both north and south is similar to that of the main oval, and dramatic variations in the filter color ratio of the main ovals have not been observed with time or longitude. The most striking variation in the filter color ratio has been for the diffuse emissions poleward of the northern main oval, which appear to have systematically brighter short wavelength emissions compared with the other emission regions. This may be interpreted as indicating brighter H Ly α emissions poleward of the main oval, since the observed ratio is greater than expected for the uabsorbed emission spectrum of electron excitation of H_2. This in turn, suggests some combination of lower energy primary particles and/or a higher H / H_2 number density ratio in the polar atmosphere compared with the main oval, coupled with the uncertainty in local variation of the atmospheric structure.

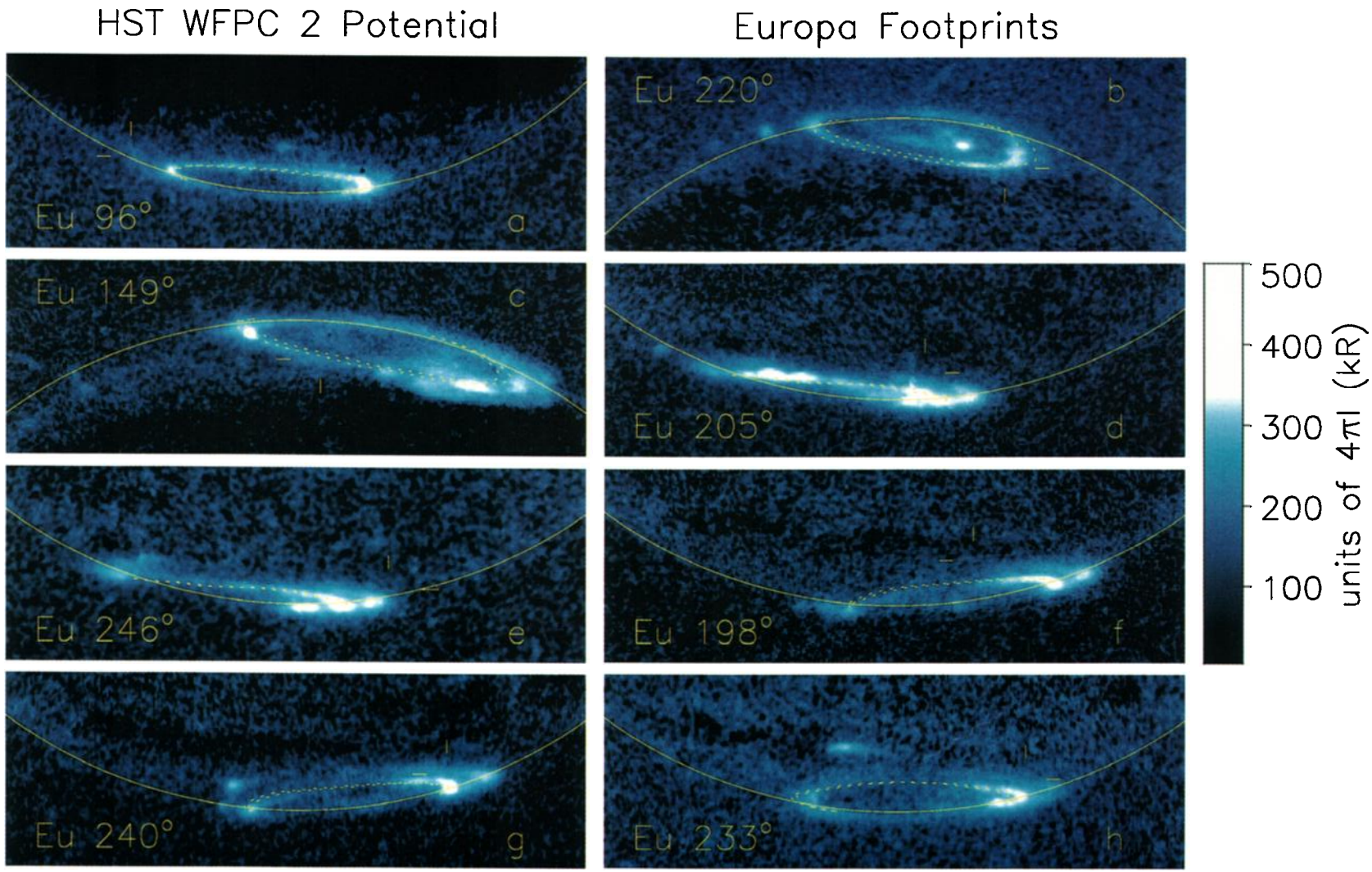

Plate 5. Images of Jupiter's aurora at times when Europa's magnetic footprint was visible from Earth, and no other satellite was within 30^0 of its orbital longitude. In each frame, the location of Europa's magnetic footprint from the VIP4 magnetic field model is indicated by tick marks. The panel letters correspond to the more detailed image information listed in Table 4, with the orbital longitude of Europa also printed in each panel. Plate 5d shows the most likely detection of auroral emission from a Europa magnetic footprint.

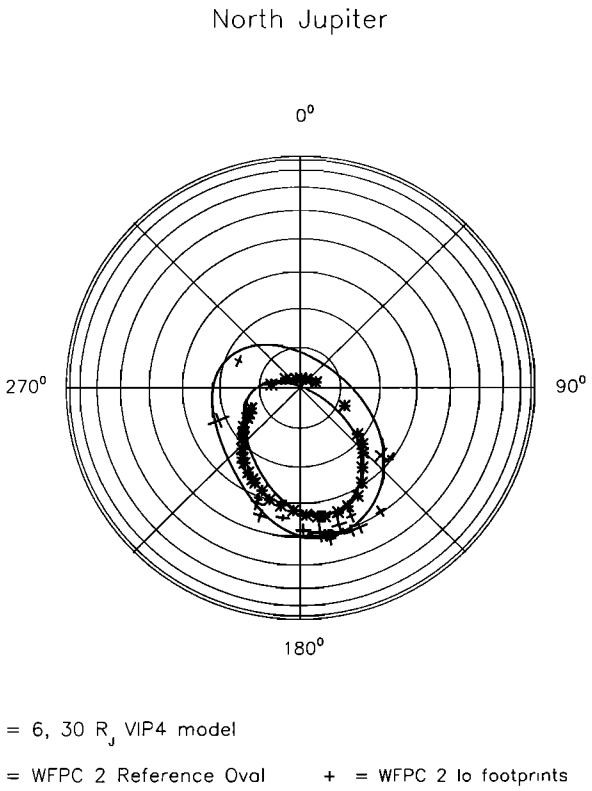

Figure 2a. North pole projections showing the "WFPC 2" reference auroral ovals (stars) from March 1995 overplotted with the locations of the 6 and 30 R_J ovals in the VIP4 planetary magnetic field model (solid lines). The regions where few points are plotted indicate regions appearing near the limb, where the model ovals are more uncertain. Crosses indicate the location of Io footprint emissions, with the lengths of the lines indicating measurement uncertainties.

3.1. Auroral Morphology

Several earlier reported features of Jupiter's aurora [*Clarke et al.*, 1996; *Ballester et al.*, 1996] are confirmed in these images, and their repetitive nature is seen in more detail or covering a longer time period. One such feature is the apparent motion of part of the northern oval from locations clearly poleward of the reference oval while in the local morning sector, to locations along the reference oval in the late afternoon sector (first reported by *Ballester et al.* (1996), which we call the "equatorward surge." The observed motion seems to be limited to the longitude range 140-180^0, although this may be due in part to the observing geometry. The extent of the emissions poleward of the reference oval can be seen in Plate 2a, panels d, f, k, and l, which range over CML = 112-132^0. Intermediate situations, with these emissions broadened and extending down toward the reference oval, are seen in Plate 2b, panels d and h, with CML = 142-151^0. Finally, the main oval emission brightening along the reference oval is seen in Plate 2a panels a and e and Plate 2b panels a and b, with CML = 185-238^0. Further examples of the motion are seen in Plates 3g and 3h. No comparable equatorward surge has been observed in the southern aurora, although a conjugate southern motion over longitudes of 140-180^0 would not be seen due to the limited viewing geometry from Earth (Plate 3). An earlier suggestion has been made that the local time effects in Jupiter's auroral distribution might be related to Jupiter's diurnal magnetospheric dynamics [*Clarke et al.*, 1996; *Ballester et al.*, 1996] following the model of Vasyliunas (1983), but it is not yet clear why the equatorward motion should be limited to the longitude range of 140-180^0, or to the magnetic field geometry in this sector. Another caveat to this suggestion is that the magnetic local time at these longitudes does not change nearly as much as the local time of the emissions, due to the geometry of Jupiter's magnetic field. A more detailed comparison of the images with models for Jupiter's magnetospheric dynamics will be needed to understand the production of the equatorward surge.

3.2. Jovian Rotation

A series of six images covering 8 hours (nearly one Jovian rotation) on June 24, 1996 is shown for both the north and south aurora in Plate 3. The character of the auroral emissions was very different in this

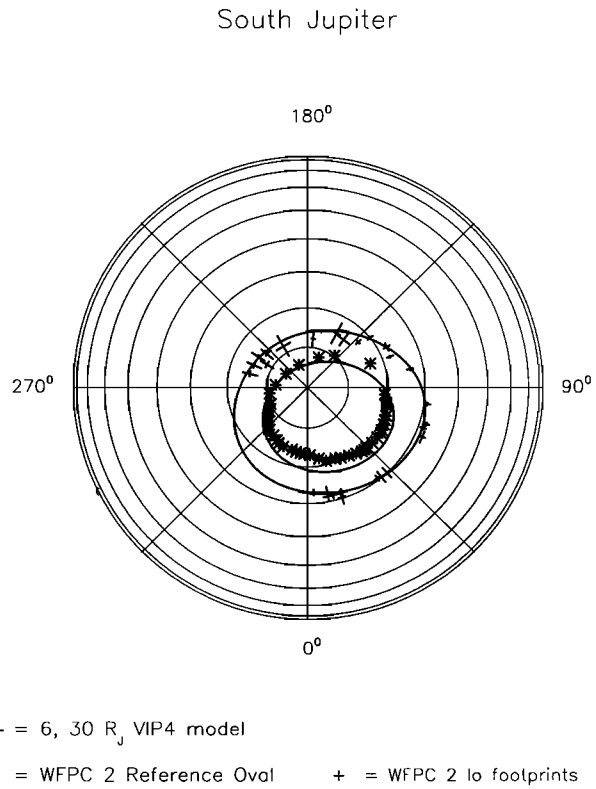

Figure 2b. South pole projections showing the "WFPC 2" reference auroral ovals (stars) from March 1995 overplotted with the locations of the 6 and 30 R_J ovals in the VIP4 planetary magnetic field model (solid lines). The regions where few points are plotted indicate regions appearing near the limb, where the model ovals are more uncertain. Crosses indicate the location of Io footprint emissions, with the lengths of the lines indicating measurement uncertainties.

time series than in the one earlier rotation observed on May 31, 1994 [*Ballester et al.,* 1996], at which time dramatic changes in the auroral morphology were seen in each of three consecutive HST orbits, including "sausage-link" patterns of six to eight bright spots along the main ovals and the evolution of a dawn storm. While no other sausage-link patterns of emission have been observed since May 1994, the apparent beginning of a dawn storm brightening was observed on June 23, 1996 (see Plate 2a, panel a), as discussed below. By contrast with the May 1994 sequence of images, it can be seen in Plate 3 that Jupiter's north and south aurora on June 24, 1996, appeared to vary little in morphology while corotating with the planet, except for the "equatorward surge" observed in the north. In addition, in all panels in Plate 3 the dusk ansae of the main ovals appear systematically brighter than the dawn ansae, an effect which is more striking in the south than in the north. While the southern aurora has a more edge-on observing geometry than the north, and limb brightening is known to enhance the apparent auroral brightness in this foreshortened geometry, in Plates 3f, 3i, and 3j the geometry is similar for the dawn and dusk ansae, while the dusk auroral emission appears brighter than that at dawn. More detailed modeling of the auroral curtain may reveal the fractional brightening required by these images. For now, it is sufficient to state that at that time there existed an auroral activity pattern in local time that led to consistently brighter emissions in the dusk sector. Other apparent local time asymmetries in Jupiter's auroral X ray emission have been reported [*Gladstone et al.,* 1998], although it is not yet clear how these might relate to the persistent dusk brightening reported here.

3.3. Dawn Storms

Another striking feature of the May 1994 time series of images was the development of a bright auroral emission above local dawn in both the north and south auroras, beginning from faint emission and growing to a brightness of several mega-Rayleighs (1 kilo-Rayleigh (kR) = 10^9 photons/cm^2 s into 4π steradians) in about 1 hour [*Ballester et al.,* 1996]. As seen in Plates 2-4, typical brightnesses of Jupiter's auroral features are several hundred kilo-Rayleighs, so that this "dawn storm" emission grew to a level many times brighter than the other features, and (on May 31, 1994) it also remained near dawn in magnetic local time while the rest of the auroral oval pattern corotated with Jupiter. This local time dependence is in contrast to most other auroral features, which either corotate with Jupiter or with Io, suggesting a different physical process leading to the production of the dawn storm. Earlier HST faint object camera (FOC) imaging had shown a similar very bright emission above local dawn in July 1993 [Gérard et al., 1994], and IUE spectra in 1990 indicated the presence of an unusually bright auroral emission generally on the approaching side of the planet [*Livengood et al.,* 1992; *Prangé et al.,* 1993], which based on its brightness, is believed to have also been a dawn storm. A dawn auroral storm with similar characteristics has also been observed in Saturn's UV aurora [*Trauger et al.,* this issue]. In Plate 2a, panel a, one can see a distinct bright emission above the dawn sector on June 23, 1996, and the location and brightness of this emission in comparison with the other images suggest that it was likely the initial development of a dawn storm. This presents a unique opportunity for the field and particle instruments on the Galileo orbiter to investigate the origin of these local-time dependent auroral storms, since at this time the Galileo orbiter was above Jupiter's dawn sector at a distance of 48 R_J from the planet.

To further investigate the morphology of these emissions (Table 2), we have re-projected the HST images from July 17, 1993, May 31, 1994, and June 23, 1996 to a common view looking down on the north polar region from above the central meridian and latitude of $+60^0$ (Plate 4). Although these images were taken years apart, the three bright emissions all appear generally along the reference oval, with different extensions along the oval and a resolved but narrow width in latitude. The measured full widths at half maximum (FWHM) in latitude of the emission at the brightest point in the three images in Plate 4 are 2200, 2500, and 1200 km. In these few measurements, the FWHM increases with the increasing brightness of the emission, as was also seen individually in the case of the observed brightening of the May 1994 storm [*Ballester et al.,* 1996]. The locations of magnetic local times are also overplotted as hash marks in Plate 4, and it can be seen that the dawn storm emissions always overlap the location of magnetic dawn along the reference oval. Note that there is a growing uncertainty in the projection accuracy as one nears the dawn limb, as can be seen from the increasingly pixelized appearance of the auroral emission.

Table 2. HST UV Images of Dawn Auroral Storms on Jupiter

Date	UT	FOC/WFPC 2 Obsroot	Jupiter CML, deg	Io OLG, deg	Europa OLG, deg	Ganymede OLG, deg	Callisto OLG, deg	Plate 4 Panel
July 17, 1993	0348	x1g30301	160.1	325.1	243.7	114.5	116.8	a
May 31, 1994	1545	u2eq010a	199.9	308.7	104.8	272.2	119.1	b
June 23, 1996	1501	u3b10302	210.7	304.7	149.5	342.4	116.0	c

FOC images begin with "x," and WFPC 2 images begin with "u". CML is System III longitude of the central meridian, and OLG is orbital longitude from superior orbital conjunction, each for the midpoint of the exposure.

The appearance of the dawn storm emissions along the reference oval implies an origin of the storm process in Jupiter's middle magnetosphere. The location fixed above magnetic dawn might imply a solar wind related process; however, no significant change in solar wind activity was found to accompany the May 1994 storm [*Ballester et al.,* 1996]. The local time dependence might also reflect the fast rotational dynamics of Jupiter's middle magnetosphere, generally at or beyond the orbit of Ganymede and connected to the current sheet [*Vasyliunas,* 1983], and some internal variability leading to the storm onset, a possibility which seems more likely. One additional note, with reference to Table 2, is that the orbital longitudes of the Galilean satellites at the times of the three dawn storms show that Io was between 305 and 325^0 on each occasion, and one or two of the other satellites were within 30^0 of dawn in orbital longitude on each occasion. We find no particular significance to the repeated location of Io on the other side of the planet. The location of one or more of the other satellites near local dawn, when combined with the apparent magnetic mapping to the middle magnetosphere, might, however, indicate some causal relation, for example, some sort of "triggering" effect provided by the other satellites to the corotating magnetodisk. This possibility should be explored with more observations to establish if the orbital locations of the satellites really determine the onset of the dawn storms.

3.4. Io Footprint

The Io footprint auroral emission has now been detected in UV images since May 1994, and in IR H_3^+ emissions since January 1992, so that we have accumulated a several year record of the locations of this emission feature in both the north and south aurora. While some longitudinal lead or lag of the emission is expected with respect to the instantaneous magnetic footprint of the satellite Io, it is believed that the latitude of the observed auroral emission in Jupiter's atmosphere should indicate the magnetic tracing of the satellite to the planet. The observed footprint emission latitudes then provide information about the near-Jupiter geometry of the magnetic field near the polar regions. Under this assumption, a revised model for Jupiter's magnetic field has been derived [*Connerney et al.,* 1998], called the VIP4 model for the input parameters, Voyager magnetometer data, Io footprint auroral latitudes, and Pioneer magnetometer data, with a fourth-order fit to these data. We present a comparison of the VIP4 model with the observed locations of the reference ovals and the Io footprint emissions in Figure 2. The 6 R_J magnetic field tracing passes through most of the Io footprint positions both north and south, as it has been constrained to do in the VIP4 model. With this new model, the reference ovals give a better fit to the 30 R_J magnetic tracing than with earlier magnetic field models, although there are still significant deviations from that model oval. Within the uncertainty in the VIP4 model and observations, we estimate that magnetic tracings exceeding 15 R_J would give plausible fits to the locations of the reference ovals at different longitudes, implying a similar range of locations in Jupiter's magnetosphere where the main auroral processes might occur. We note that this range includes the distance at which the Galileo magnetometer has found the Jovian magnetodisk to abruptly change its thickness [*Kivelson et al.,* 1997].

In the Alfven wing model of *Goldreich and Lynden-Bell* (1969), electric currents driven by Io, acting as a unipolar inductor, perturb the local magnetic field and direct the current-carrying field lines and resulting footprint emission forward in the corotation direction with respect to the unperturbed magnetic field. This corresponds to smaller longitudes both north and south and is referred to as the emission "leading" the unperturbed magnetic footprint, i.e. in the direction of the corotating magnetic field. The proposed current was initially assumed to pass quickly between Io and Jupiter, setting up a direct current loop, so that the observed lead of the footprint emission would indicate the degree of magnetic field perturbation near Io. After the Voyager measurements of Io's plasma torus, it was proposed that the currents were carried by Alfven waves, with a finite propagation time between Io and Jupiter's ionosphere which depended, in part, on the density of the torus plasma along the path to Jupiter's atmosphere [*Goertz,* 1980; *Neubauer,* 1980]. In this case, the footprint emission would also be expected to lead the unperturbed magnetic footprint, but with an angle corresponding to the time delay of the Alfven waves to propagate down to Jupiter's atmosphere [*Belcher,* 1987]. A hybrid model has also been proposed [*Crary and Bagenal,* 1997] in which the interaction begins as an Alfvenic disturbance near Io, and evolves into a steady current loop as it moves downstream. Measurements of the lead angle of the footprint emissions, and any systematic variations with Io's location above or below the plasma torus, could potentially discriminate between these models for the current flow and interaction between Io and Jupiter's ionosphere.

In Figure 3 we show the apparent lead or lag of the observed Io footprint auroral emissions with respect to the instantaneous magnetic field in both the O6 [*Connerney,* 1992] and VIP4 magnetic field models. The comparison with the O6 model shown in Figure 3 includes a much larger data set than previously presented, now covering over 3 years time, and within the uncertainty in measurement the lead/lag pattern appears to be stable with time with characteristic and different patterns in the north and south. The observed lead/lag angles, however, are mainly within the 8-10^0 uncertainty in the O6 model, making an interpretation difficult. It is interesting to note that in comparison with the VIP4 model, the emission appears to lead the instantaneous magnetic footprint (within the error bars) in the plasma flow direction by 0-15^0 at all longitudes in both the north and south. While there still remains a significant uncertainty of several degrees in the VIP4 model, it now appears more likely that the emission occurs generally

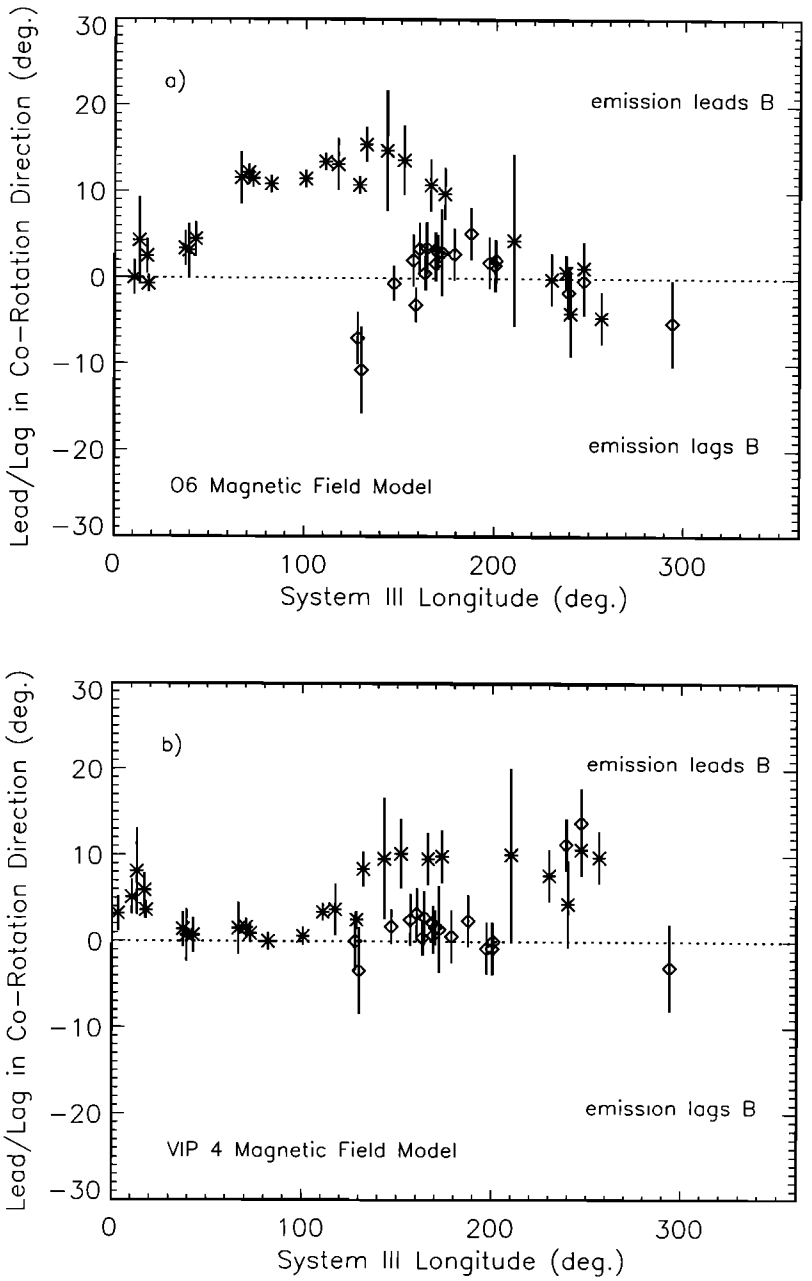

Figure 3. Comparison of lead/lag angles of the observed Io magnetic footprint auroral emission from the instantaneous mapping of the magnetic field (a) for the O6 model magnetic field and (b) for the VIP 4 magnetic field model. Stars represent measured footprint locations in the south, diamonds in the north, and the verticle lines indicate uncertainties in the measured emission locations: no uncertainties are plotted for the magnetic field models. The figure includes all observations from May 1994 through September 1997 in which the Io footprint emission appeared sufficiently far from the limb (typically 10-15^0) for an accurate measurement of its location. In the Alfven wing model of Goldreich and Lynden-Bell, electric currents near Io perturb the local magnetic field and direct the current-carrying field lines and resulting footprint emission forward in the corotation direction with respect to the unperturbed magnetic field. This corresponds to smaller longitudes both north and south, plotted as "emission leads B" in this figure.

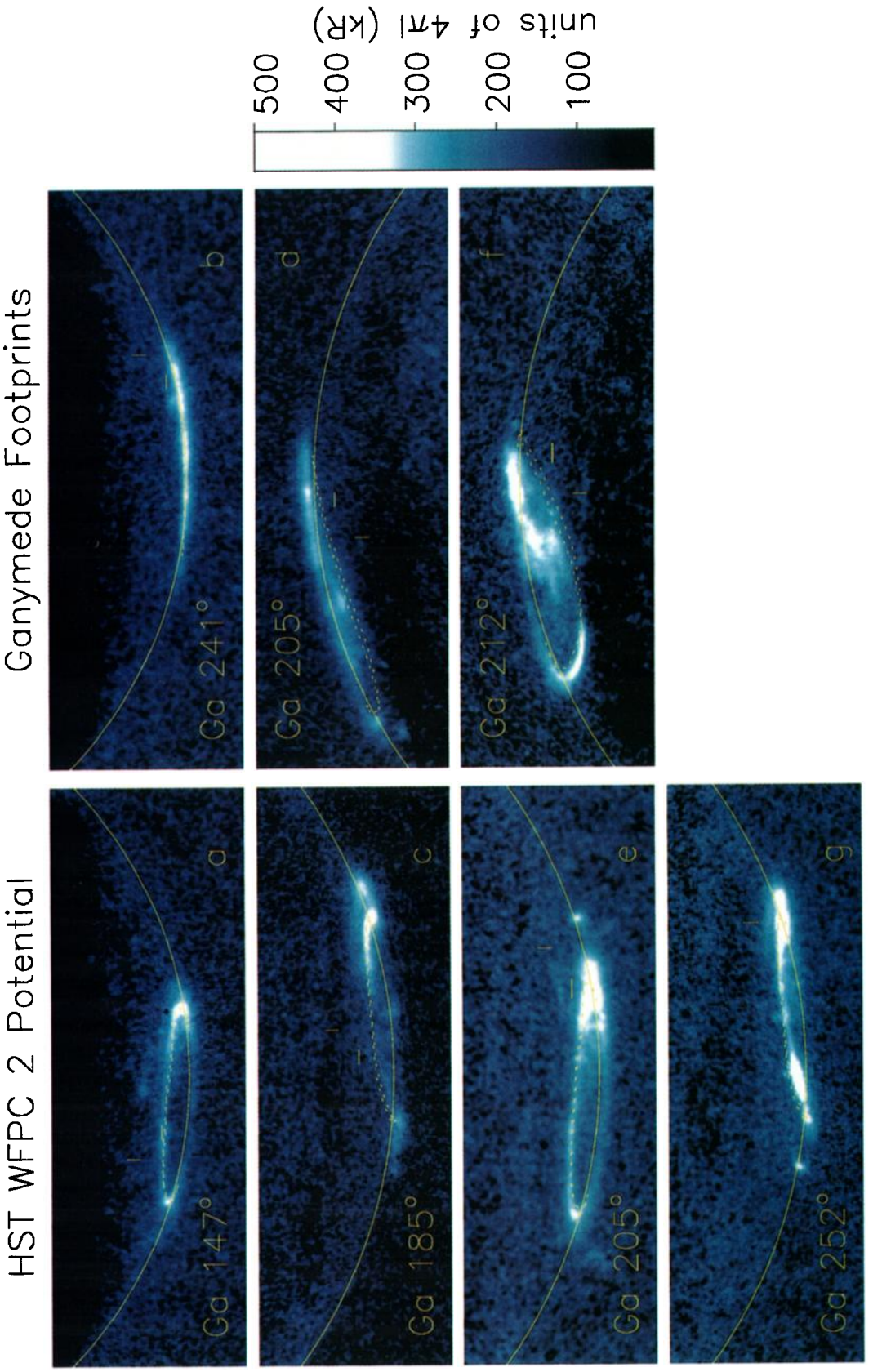

Plate 6. Images of Jupiter's aurora at times when Ganymede's magnetic footprint was visible from the Earth, and no other satellite was within 30^0 of its orbital longitude. In each frame, the location of Ganymede's magnetic footprint from the VIP4 magnetic field model is indicated by tick marks. The panel letters correspond to the more detailed image information listed in Table 5, with the orbital longitude of Ganymede also printed in each panel. Plate 6b shows the most likely detection of auroral emission from a Ganymede magnetic footprint. The feature on the dusk limb in Plate 6e is the Io footprint.

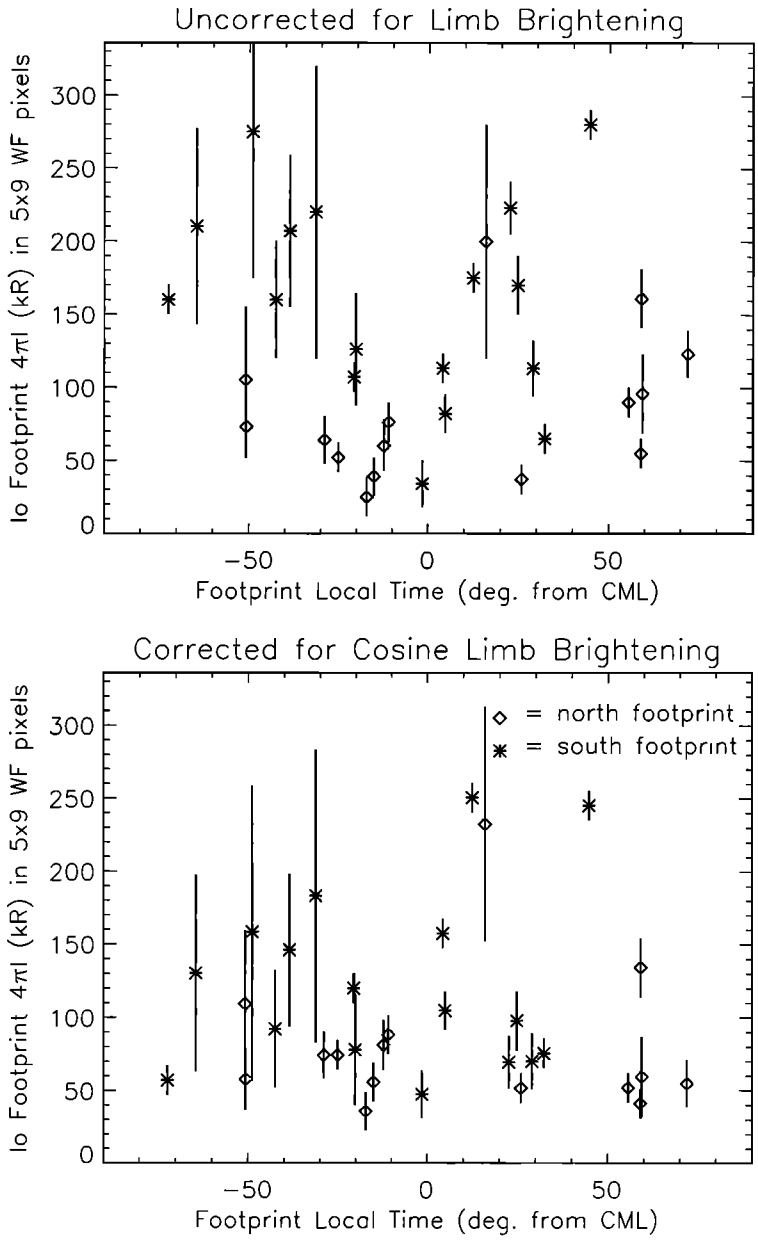

Figure 4. Brightness of Io footprint emissions in a 0.5 x 0.9 arc sec area versus local time (a) measured in degrees of longitude from the central meridian. Like Figure 3, stars indicate southern points and diamonds northern points, with vertical lines for the measurement uncertainties. (b) Effect of correcting for an assumed cosine limb brightening with respect to a reference location at 67^0 latitude on the central meridian.

downstream of the instantaneous magnetic footprint in the corotation direction by a value in the range of 0-15^0. Jupiter's rotation with an inclined and asymmetric magnetic field causes the torus to move north/south with respect to Io, thereby varying the current path length through the torus with longitude oppositely in the north and south. The observed southern lead angles with the VIP4 model appear close to 0^0 when Io is above 0-50^0 longitude, and therefore south of the torus with a minimum column of torus plasma toward the south pole. The largest southern lead angles are seen over 120-240^0, when Io is generally north of the torus with maximum columns of plasma toward the south pole. The northern points do not cover as broad a range of longitudes, but the cluster of points near 0^0 lead angles over 140-200^0 sub-Io longitude is also consistent with a minimum column of torus plasma toward the north pole. Within the remaining uncertainty in the VIP4 model, these trends appear consistent with the picture of an Alfvenic disturbance near Io.

In addition to the changing lead angle, any variation in the electric current between the north and south footprint auroral emission regions (which depends on the changing columns of torus plasma) might appear

as changes in the auroral footprint brightness. However, there are other factors which may affect the auroral brightness. For one, the magnetic field strength (and corresponding electric potential) at Io varies by 20% with longitude. The field strength at the north and south poles in Jupiter's atmosphere also varies by more than a factor of 2, depending on the sub-Io longitude, with corresponding variations in the sizes of the loss cones for an assumed pitch angle distribution of trapped charged particles. Lacking detailed knowledge of the nature of the electric current linking Io with Jupiter's ionosphere, we have simply searched for correlations between the auroral footprint brightness with various parameters, including time, local time, and sub-Io longitude in the north and south. We begin in Figure 4 by plotting the average Io footprint emission brightness in a 5 x 9 pixel area (0.5 x 0.9 arc sec) versus local time of the footprint given by the difference in longitude from the central meridian. The error bars in Figures 4 and 5 have been determined by the standard deviation in brightness obtained with measurements shifted by +/- one pixel in longitude and latitude. These error bars indicate the sensitivity of the measured brightness to the detector noise level and other nearby emissions, rather than the uncertainty in the absolute calibration. We interpret the trend of increasing brightness away from the central meridian in the upper panel of Figure 4 as the expected limb brightening of the optically thin auroral emissions. We have then corrected the emission brightnesses for an assumed cosine limb brightening (i.e., converted to the expected brightness if the feature were on the central meridian at 67^0 latitude), plotted in the lower panel of Figure 4. In this case, there are no longer any clear trends with local time, but there is a substantial degree of variation in brightness.

The brightnesses are then plotted versus time in Figure 5, and also versus sub-Io longitude for the entire data set and for the single Jovian rotation images on June 24, 1996. The variability with time is clear from Figure 5, and there is also considerable scatter in the data versus sub-Io longitude. There might be some trends with longitude, for example, an increase in southern brightness when Io passes $60\text{-}70^0$ longitude or in the northern brightness when Io passes 180^0 longitude. These trends appear also in the data from June 24, 1996, obtained over one Jovian rotation. The factor of 2-3 scatter in the data with time for the same footprint and sub-Io longitude, however, prevents us from identifying any clear trends in the data at this time. More continuous observations like those in June 1996 would help a great deal in determining any clear trends in Io's auroral footprint brightness.

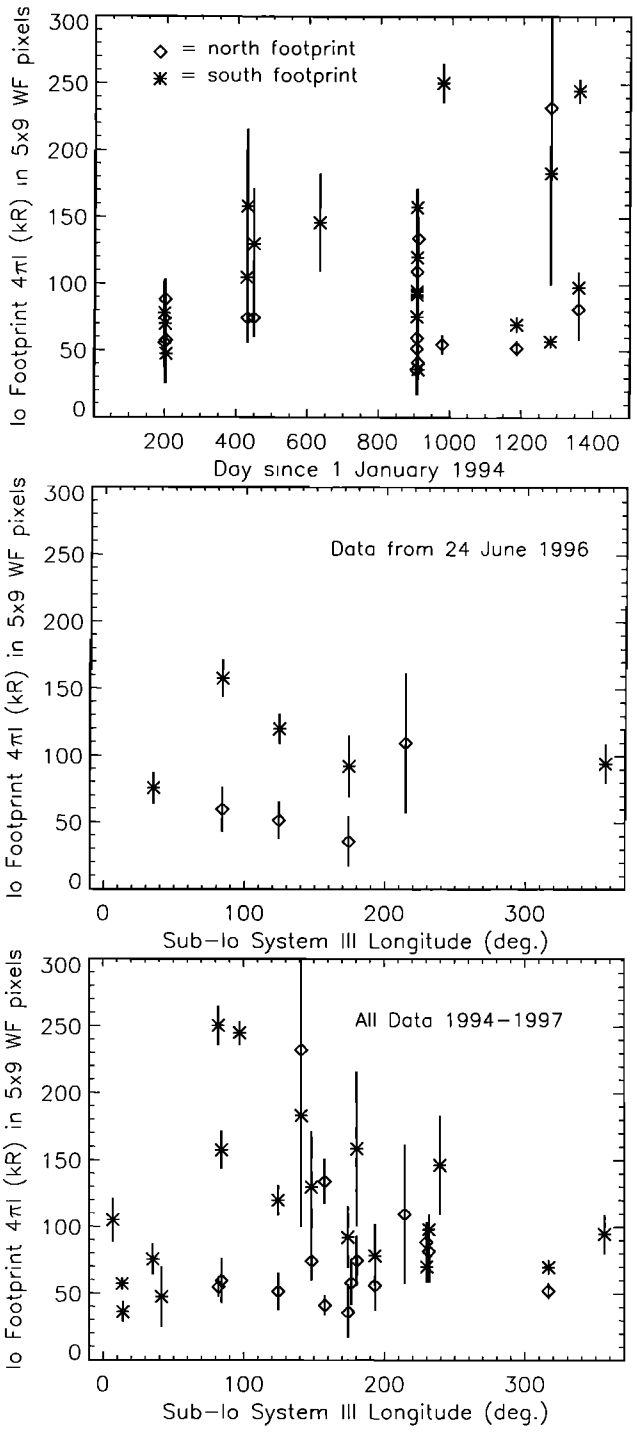

Figure 5. Brightness of Io footprint emissions plotted as in Figure 4, in all panels corrected for a cosine limb brightening, and plotted (a) versus time, (b) data from June 24, 1996 versus sub-Io longitude, and (c) all data versus sub-Io longitude.

3.5. Other Satellite Footprint Aurora

In addition to the electric potential generated at Io by its motion with respect to Jupiter's magnetic field, potentials will develop by the same process radially across the other Galilean satellites. Estimates of these potentials are listed in Table 3, and while they are progressively less for the more distant satellites, they are still quite substantial. The generation of an Io-like electric current linking the other satellites with Jupiter's ionosphere would also require an electrically conducting satellite, with associated uncertainties, and no correlations of the orbital locations of any other satellite with Jupiter's decametric radio emissions have been reported

Table 3. Estimates of Potentials Across the Galilean Satellites

Satellite	Diameter, km	$\mathbf{B}_J$ Speed, km/s	$\|\mathbf{B}_J\|$, nT	EMF, kV
Io	3630	57	1800	370
Europa	3140	106	440	150
Ganymede	5260	179	110	100
Callisto	4800	200	33	30

Electromotive force (EMF) across the diameter of each satellite was estimated from the change in magnetic flux with time, using measured values of the magnetic field strength during the Galileo encounters (K. Khurana, personal communication, 1997) and corotation speed near each satellite.

[*Carr et al.*, 1983]. A more sensitive detection technique might be the observation of auroral emission from the satellite footprints, and we report here an initial search for such footprint emissions. We have confined our search to Europa and Ganymede, since Callisto's footprint is so close to the main oval that we would not expect to be able to distinguish such an emission, and we have not observed any emissions equatorward of the locus of Io footprint emissions where emission from Amalthea would occur. The images searched, listed in Tables 4 and 5, were selected for times when each satellite was on the Earth-facing side of Jupiter and when no other satellites were within roughly 30^0. These images are shown in Plate 5 for Europa and Plate 6 for Ganymede.

In Plate 5 there are cases, as in Plates 5a, 5c, and 5f, when there is no auroral emission near the expected location of Europa's magnetic footprint. The best evidence for a Europa footprint emission appears in Plate 5d, in which there is a small bright feature somewhat poleward and to the left of the VIP4 model location. This feature is small and just outside the main oval, as expected for the magnetic tracing from Europa. There also appears some emission equatorward of the main oval in Plate 5e, but similar emission appears in Plate 5f when Europa is much closer to the central meridian. Overall, the images do not show consistent emission from the expected Europa footprint locations, while the feature in panel d of Plate 5 appears closest to what one would expect for a Europa footprint. As a criterion for associating such a footprint emission with another satellite, we recommend that observations be made in which the motion of the suspected emission feature can be seen to remain under the satellite while other auroral emissions corotate with Jupiter, as has been done with Io's footprint.

Plate 6 shows the images in which Ganymede's auroral footprint might appear, with the same format as Plate 5 for Europa. Again, there are clear cases where no emissions appear close to the expected location of Ganymede's magnetic footprint, including Plates 6a, 6c, 6d, and 6f. The best evidence for Ganymede footprint emission is in Plate 6b, with a clear emission feature just equatorward of the main oval to the left of the expected location. In fact, this emission's location was first measured assuming that it was an Io footprint, and only after it appeared clearly poleward of the other Io footprints was it realized that it was close to Ganymede's location and not Io's. As for Europa, however, the observation of an emission remaining fixed under the satellite will be key to demonstrating that such an emission is linked to that satellite.

Summary

UV images of Jupiter's aurora are presented, obtained with the HST WFPC 2 instrument close in time to in situ measurements of the Jupiter system by the Galileo orbiter. The morphology of the auroral emissions is presented, including a comparison with two different magnetic field models for the magnetic mapping of the emissions into Jupiter's magnetosphere, oc-

Table 4. HST/WFPC 2 Images of Potential Europa Footprints

Date	UT	WFPC 2 Obsroot	Jupiter CML, deg	Europa OLG, deg	Panel in Plate 5
March 4, 1995	2310	u2mu0402	5.7	96.9	a
March 9, 1995	1725	u2n20302	190.3	220.8	b
June 23, 1996	1501	u3b10302	210.7	149.5	c
June 24, 1996	0354	u3b10202	318.6	205.0	d
June 24, 1996	1344	u3b10102	314.3	246.9	e
June 27, 1996	1534	u3b10502	113.4	198.7	f
June 28, 1996	0114	u3b10602	104.0	240.1	g
Sept. 3, 1996	0938	u3fw0502	58.1	233.3	h

CML is System III longitude of the central meridian, and OLG is orbital longitude from superior orbital conjunction, each for the midpoint of the exposure.

Table 5. HST/WFPC2 Images of Potential Ganymede Footprints

Date	UT	WFPC 2 Obsroot	Jupiter CML, deg	Ganymede OLG, deg	Panel in Plate 6
March 4, 1995	2310	u2mu0402	5.7	147.8	a
March 6, 1995	2015	u2mu0502	201.0	241.8	b
June 27, 1996	1534	u3b10502	113.4	185.2	c
Juen 28, 1996	0114	u3b10602	104.0	205.5	d
Sept. 7, 1996	1144	u3fw0202	16.1	205.6	e
Sept. 7, 1996	0938	u3fw0302	132.8	212.4	f
Sept. 8, 1996	1014	u3fw0402	112.2	252.7	g

CML is System III longitude of the central meridian, and OLG is orbital longitude from superior orbital conjunction, each for the midpoint of the exposure.

casional "dawn storms", and a persistent motion in the northern aurora called the "equatorial surge". An extended set of observations of Io's footprint auroral emissions is presented, and compared with the instantaneous magnetic field mapping as well as time variations in the emission brightness. Finally, a search is presented for footprint emissions connected to Europa and Ganymede.

Acknowledgments. This work is based on observations with the NASA/ESA Hubble Space Telescope, obtained at the Space Telescope Science Institute (ST ScI), which is operated by AURA, Inc., for NASA under contract NAS5-26555. This work was supported by NASA under contract JPL 959122 and grants GO-5828.01-94A and GO-6743.01-95A from ST ScI to the University of Michigan.

References

Ajello, J.M., et al., Galileo orbiter ultraviolet observations of Jupiter's aurora, *J. Geophys. Res.*, this issue.

Ballester, G.E., et al., Time-resolved observations of Jupiter's far-UV aurora: Comparison of WFPC2 and IUE, *Science, 274,* 409-413, 1996.

Baron, R., R.D. Joseph, T. Owen, J. Tennyson, S. Miller, and G.E. Ballester, Imaging Jupiter's aurorae from H_3^+ emissions in the 3-4 μm Band, *Nature, 353,* 539-542, 1991.

Belcher, J.W., The Jupiter-Io connection: An Alfven engine in space, *Science, 238,* 170-176, 1987.

Broadfoot, A.L., et al., Extreme ultraviolet observations from Voyager 1 encounter with Jupiter, *Science, 204,* 979-982, 1979.

Caldwell, J., A.T. Tokunaga, and F.C. Gillett, Possible infrared aurora on Jupiter, *Icarus, 44,* 667-675, 1980.

Caldwell, J., R. Halthore, G. Orton, and J. Bergstralh, Infrared polar brightenings on Jupiter, IV, Spatial properties of methane emission, *Icarus, 74,* 331-339, 1988.

Caldwell, J., B. Turgeon, and X.M. Hua, Hubble Space Telescope imaging of the north polar aurora on Jupiter, *Science, 257,* 1512-1515, 1992.

Carr, T.D., M.D. Desch, and J.K. Alexander, Phenomenology of magnetospheric radio emissions, in *Physics of the Jovian Magnetosphere,* edited by A.J. Dessler, pp. 226-284, Cambridge Univ. Press, New York, 1983.

Clarke, J.T., H.W. Moos, S.K. Atreya, and A.L. Lane, Observations from Earth orbit and variability of the polar aurora on Jupiter, *Astrophys. J. Lett., 241,* L179-L182, 1980.

Clarke, J.T., J. Caldwell, T. Skinner, and R. Yelle, The aurora and airglow of Jupiter, Time Variable Phenomena in the Jovian System, *NASA Spec. Publ., SP-494,* 211-220, 1989.

Clarke, J.T., J. Trauger, J. Holtzman, and the WFPC 2 Science Team, Far-ultraviolet imaging with the Hubble Space Telescope Wide Field Planetary Camera 2, in *Calibrating Hubble Space Telescope,* edited by A. Koratkar and C. Leitherer, p. 322-333, Space Telescope Sci. Inst., Baltimore, MD, 1995a.

Clarke, J.T. et al., Hubble Space Telescope far-ultraviolet imaging of Jupiter during the impacts of Comet Shoemaker-Levy 9, *Science, 267,* 1302-1307, 1995b.

Clarke, J.T. et al., Far-UV imaging of Jupiter's aurora with HST/WFPC 2, *Science, 274,* 404-409, 1996.

Connerney, J.E.P., Doing more with Jupiter's magnetic field, in *Planetary Radio Emission,* vol. 3, edited by H. Rucker, M.L. Kaiser, and S.J. Bauer, pp.13-33, Austrian Acad. of Sci. Press, Vienna, 1992.

Connerney, J.E.P., R. Baron, T. Satoh, and T. Owen, Images of excited H_3^+ at the foot of the Io flux tube in Jupiter's atmosphere, *Science, 262,* 1035-1038, 1993.

Connerney, J.E.P., T. Satoh, and R.L. Baron, Interpretation of auroral "lightcurves" with application to Jovian H_3^+ emissions, *Icarus, 122,* 24-35, 1996.

Connerney, J.E.P., M.H. Acuna, N.F. Ness, and T. Satoh, New model of Jupiter's magnetic field constrained by the Io flux tube footprint, *Icarus,* in press, 1998.

Crary, F.J., and F. Bagenal, Coupling the plasma interaction at Io to Jupiter, *Geophys. Res. Lett., 24,* 2135-2138, 1997.

Dols, V., J.C. Gérard, F. Paresce, R. Prangé, and A Vidal-Madjar, Ultraviolet imaging of the Jovian aurora with the Hubble Space Telescope, *Geophys. Res. Lett., 19,* 1803-1806, 1992.

Drossart, P., B. Bezard, S.K. Atreya, J. Lacy, E. Serabyn, A. Tokunaga, and T. Encrenaz, Enhanced acetylene emission near the north pole of Jupiter, *Icarus, 66,* 610-618, 1986.

Drossart, P., Detection of H_3^+ on Jupiter, *Nature, 340,* 539-541, 1989.

Drossart, P., R. Prangé, and J.-P. Maillard, Morphology of infrared H_3^+ emissions in the auroral regions of Jupiter, *Icarus, 97,* 10-25, 1992.

Gérard, J.C., V. Dols, F. Paresce, and R. Prangé, Morphology and time variation of the Jovian far UV aurora: Hubble Space Telescope observations, *J. Geophys. Res., 98,* 18,793-18,801, 1993.

Gérard, J.C., et al., A remarkable auroral event on Jupiter observed in the ultraviolet with the Hubble Space Telescope, *Science, 266,* 1675-1678, 1994.

Gladstone, G.R., J.H. Waite Jr., and W.S. Lewis, Secular and local time dependence of Jovian X ray emissions, *J. Geophys. Res.*, this issue.

Goertz, C.K., Io's interaction with the magnetosphere, *J. Geophys. Res., 85*, 2949-2954, 1980.

Goldreich, P., and D. Lynden-Bell, Io, a Jovian unipolar inductor, *Astrophys. J., 156*, 59-78, 1969.

Grodent, D., V. Dols, and J.C. Gérard, The equatorial boundary of the ultraviolet Jovian north aurora observed with multispectral Hubble Space Telescope images, *J. Geophys. Res., 101*, 2163-2168, 1996.

Harris, W.M., J.T. Clarke, M.A. McGrath, and G.E. Ballester, Analysis of Jovian auroral H Ly-α emission (1981-1990), *Icarus, 23*, 350-365, 1996.

Holtzman, J., et al., The performance and calibration of the WFPC 2, *Publ. Astron. Soc. Pac., 107*, 156-178, 1995.

Kim, S.J., P. Drossart, J. Caldwell, J.P. Maillard, T. Herbst, and M. Shure, Images of aurora on Jupiter from H_3^+ emission at 4 microns, *Nature, 353*, 536-539, 1991.

Kim, Y.H., S.J. Kim, J.A. Stuewe, J. Caldwell, and T.M. Herbst, Jovian auroral ovals inferred from infrared H_3^+ images, *Icarus, 112*, 326-336, 1994.

Kivelson, M.G., K.K. Khurana, C.T. Russell, D.J. Southwood, and R.J. Walker, Global measurements of Jupiter's magnetic field by Galileo (abstract), *Eos Trans. AGU, 78*, Spring Meet. Suppl., S292, 1997.

Kostiuk, T., M.J. Mumma, J.J. Hillman, D. Buhl, L.W. Brown, and J.L. Faris, NH_3 spectral line measurements on Earth and Jupiter using a 10 μm superheterodyne receiver, *Infrared Phys., 1*, 431-439, 1977.

Livengood,T.A., H.W. Moos, G.E. Ballester, and R. M. Prangé, Jovian auroral activity, 1981-1991, *Icarus, 97*, 26-45, 1992.

Metzger, A., D.A. Gilman, J.L. Luthey, K.C. Hurley, H.W. Schnopper, F.D. Seward, and J.D. Sullivan, The detection of X rays from Jupiter, *J. Geophys. Res., 88*, 7731-7741, 1983.

Neubauer, F.M., Nonlinear standing Alfven wave current system at Io: Theory, *J. Geophys. Res., 85*, 1171-1181, 1980.

Prangé, R., P. Zarka, G.E. Ballester, T.A. Livengood, L. Denis, T. Carr, F. Reyes, S.J. Bame, and H.W. Moos, Correlated variations of UV and radio emissions during an outstanding Jovian auroral event, *J. Geophys. Res., 98*, 18,779-18,791, 1993.

Prangé, R., et al., Auroral signature of Comet Shoemaker-Levy 9 in the Jovian magnetosphere, *Science, 267*, 1317-1320, 1995.

Skinner, T.E., S.T. Durrance, P.D. Feldman, and H.W. Moos, IUE observations of longitudinal and temporal variations in the Jovian auroral emission, *Astrophys. J., 278*, 441-448, 1984.

Trafton, J.T., D.F. Lester, and K.L. Thompson, Unidentified emission lines in Jupiter's northern and southern 2 μm aurorae, *Astrophys. J. Lett., 343*, L73-L76, 1989.

Trauger, J.T., et al., The on-orbit performance of WFPC 2, *Astrophys. J. Lett., 435*, L3-L6, 1994.

Trauger, J.T., et al., Saturn's hydrogen aurora: Wide-field planetary camera 2 imaging observations from the Hubble Space Telescope, *J. Geophys. Res.*, this issue.

Vasyliunas, V.M., Plamsa distribution and flow, in *Physics of the Jovian Magnetosphere*, edited by A. J. Dessler, pp. 395-453, Cambridge, Univ. Press, New York, 1983.

Waite, J.H., et al., ROSAT observations of the Jupiter aurora, *J. Geophys. Res., 99*, 14,799-14,809, 1994.

West, R.A., E. Karkoschka, A.J. Friedson, M. Seymour, K.H. Baines, and H.B . Hammel, Impact debris particles in Jupiter's stratosphere, *Science, 267*, 1296-1301, 1995.

Yung, Y.L., G.R. Gladstone, K.M. Chang, J.M. Ajello, and S.K. Shrivastava, H_2 fluorescence spectrum from 1200 to 1700 Å by electron impact: Laboratory study and application to Jovian aurora, *Astrophys. J. Lett., 254*, L65-L69, 1982.

J. Ajello, K. Tobiska, and J. Trauger, Jet Propulsion Laboratory, 4800 Oak Grove Drive, Pasadena, CA 91109.

G. Ballester and J. T. Clarke, Space Physics Research Laboratory, 2455 Hayward Street, University of Michigan, Ann Arbor, MI 48109-2143 (email: clarke@umich.edu)

L. Ben Jaffel, Institute for Astrophysics, 98 Bis Boulevard Arago, Paris 75014, France.

J.E.P. Connerney, NASA Goddard Space Flight Center, Code 695, Greenbelt, MD 20771.

J.-C. Gérard, Institute of Astrophysics, Avenue Cointe N 5, University of Liège, 4000 Liège, Belgium.

G. R. Gladstone and J. H. Waite Jr.,Southwest Research Institute, 6220 Culebra Road, POD 28510, San Antonio, TX 78228-0510.

W. Pryor, Laboratory for Atmospheric and Space Physics, 1234 Innovation Drive, University of Colorado, Boulder, CO 80303.

(Received October 2, 1997; revised March 22, 1998; accepted April 6, 1998.)